Energy Balance Computations of Snowmelt in a Subarctic Area

A. G. PRICE

Division of Social Sciences—Geography, University of Toronto, Scarborough College, Scarborough, Ontario, Canada

T. DUNNE

Department of Geological Sciences, University of Washington, Seattle, Washington 98195

A physically based model was used to predict daily snowmelt on 2000-m² plots in the subartic. The plots had a range of aspects and inclinations under boreal forest and on the tundra. The energy balance, computed for each of the plots, was compensated for differences in radiative and turbulent energy fluxes caused by varied slope geometry and vegetative cover. The turbulent energy fluxes were also corrected for the effects of the stable stratification of the air over the snow surface. The predictions of the model were compared with daily melts derived from runoff measured on the snowmelt plots. The results show that the method is a good predictor of daily amounts of snowmelt, although some uncertainties are introduced by changes in the snow surface during the melt period. In a companion paper we show how hourly snowmelt rates, calculated from the energy balance, can be used to predict runoff hydrographs from hillside plots.

INTRODUCTION

The prediction of daily snowmelt is of great importance in areas where accumulated snow represents much of the annual precipitation. In such situations the accurate prediction of daily melt volumes is a very desirable aid in water management and is also useful in the design of water control structures.

Snowmelt may be predicted in several ways. The simplest and longest-used method is to relate observed daily melts to accumulated degree-days [*Collins*, 1934]. Other, more complex heat indices may be used, involving more than one relevant variable; or a more sophisticated statistical analysis may be performed. [*Pysklywec et al.*, 1968; *Zuzel and Cox*, 1975]. The weakness of such methods is that their results may not be valid outside the area where the work was done.

Thus it is desirable to use a prediction method which is generally applicable. *Wilson* [1941] made an early attempt to formulate a general energy balance approach to the problem. The *U.S. Army Corps of Engineers* [1956] made a more exhaustive study and included thorough testing of predictions against field data. The physical basis of the work is sound, but some assumptions made in the development of the equations governing the turbulent exchanges are unrealistic, particularly the adoption of the exponential wind profile and the ignoring of the effects of stability.

One of the shortcomings of most earlier attempts to apply the energy balance method to snowmelt prediction is the inadequate assessment of the turbulent exchanges of energy between the air and the snow, in particular, the effects of nonneutral conditions over the snow surface on these exchanges. *Anderson* [1968], in a successful application of the energy balance method, fails to mention the problem of stability. *Fohn* [1973] also applied the energy balance to snowmelt without correcting the turbulent exchanges of heat for the effects of stability. *De la Casiniere* [1974] made a good analysis of the energy balance over a melting snowpack and showed that stable conditions predominate. He did not, however, test computed heat flows against observed melt rates.

The present paper reports the results of the application of the energy balance method to the prediction of daily snowmelt on plots in the boreal forest and tundra of subarctic Labrador. It compares daily melts computed from the energy balance with melts observed in the field. The results demonstrate that the energy balance is a good short-term predictor of snowmelt, with some uncertainties being introduced by the methods used to estimate net radiation and surface roughness. The investigation suggests that future studies of the energy balance over snow should pay particular attention to these variables.

THEORETICAL DISCUSSION

If a snowpack is isothermal at 0°C, then its heat balance may be written as

$$H_m = H_r + H_c + H_e + H_p + H_g \quad \text{cal cm}^{-2}\,\text{h}^{-1} \qquad (1)$$

where H_m is the heat available for melting snow, H_r is the net radiative heat flux, H_c is the sensible heat flux, H_e is the latent heat flux, H_p is the heat gained from precipitation, and H_g is the ground heat flow. In the period considered in the present study, no rain fell, so that H_p was zero. In addition, frozen ground at the base of the snowpack persisted throughout the melt period, so that H_g was assumed to be zero. The three remaining components, then, are as follows.

Radiation Heat Flow (H_r)

Radiation heat flow, or net all-wave radiation, is expresed as the balance of incoming and outgoing radiation:

$$H_r = (Q + q)(1 - \alpha) + L_n \quad \text{cal cm}^{-2}\,\text{h}^{-1} \qquad (2)$$

where Q represents the direct beam of solar radiation, q the diffuse fraction of solar radiation, α the shortwave reflectivity of the snow surface, and L_n the long-wave balance. Measurements of H_r can be made with a net radiometer, but it is unusual to have a continuous record of such measurements. Attempts to compute H_r rely on the fact that L_n in (1) may be written as

$$L_n = L\downarrow - L\uparrow \quad \text{cal cm}^{-2}\,\text{h}^{-1} \qquad (3)$$

where $L\downarrow$ is the sky emission and $L\uparrow$ is the emission from the

snow surface. $L\downarrow$ may be computed as a function of atmospheric temperature and vapor pressure. $L\uparrow$ may be calculated from the temperature and emissivity of the melting snow surface. If $(Q + q)$ and α are measured, then an estimate of H_r can be made. An example of this type of analysis is given by *Anderson* [1954]. There are some problems associated with this technique, relating primarily to the difficulty of using near-surface measurements to characterize the vertical distribution of air mass properties. In the present study, hourly values of L_n were computed by using a Brunt-type equation [*Brunt*, 1932] and were combined with measured values of $(Q + q)$ and α. Comparison of the computed values with measured H_r showed that the calculated values were generally inaccurate, and for the final computations, H_r was estimated by a method to be described later.

Sensible and Latent Heat Fluxes

The two remaining heat fluxes in (1) are the turbulent heat flow terms: the inputs of heat driven by gradients of temperature and moisture and by turbulence in the lower atmosphere. The equations governing these heat exchanges in neutral conditions are

$$H_c = \rho_a \cdot C_p \cdot D_h(T_a - T_s) \quad \text{cal cm}^{-2}\,\text{h}^{-1} \tag{4}$$

and

$$H_e = L \cdot \rho_a D_w \cdot (0.622/p)(e_a - e_s) \quad \text{cal cm}^{-2}\,\text{h}^{-1} \tag{5}$$

where ρ_a is the density of air, C_p is the specific heat of air at constant pressure, p is the atmospheric pressure in millibars, T_a is the air temperature in degrees Celsius, T_s is the snow surface temperature in degrees Celsius, e_a is the vapor pressure of the air in millibars, e_s is the snow surface vapor pressure in millibars, and L is the latent heat of vaporization of water in calories per gram.

The exchange coefficient for heat (D_h) and the coefficient for moisture (D_w) may be derived by analogy with the transfer of momentum, so that

$$D_h = D_w = \frac{k^2 u_z}{[\ln (z/z_0)]^2} \text{ cm h}^{-1} \tag{6}$$

In stratified conditions (either lapse or stable), however, a correction must be applied to (6), which can be either the complex Monin and Obuchov factor [*Webb*, 1965] or the simple linear Richardson number. The two corrections are essentially identical within a considerable range [*Price*, 1975], and for simplicity the Richardson number was used in the analysis that follows.

Under stable conditions, air near the surface is cooled and assumes a higher density. This air tends to maintain its position when it is disturbed by turbulence, decreasing rates of turbulent exchange. *Monteith* [1957] suggested that

$$(D_h)_s = D_h/(1 + \sigma Ri) \tag{7}$$

where $(D_h)_s$ is the transfer coefficient under stable conditions, D_h is the transfer coefficient under neutral conditions, and Ri is the Richardson number.

$$Ri = (g \cdot z \cdot \Delta T)/[T_{abs}(\Delta u)^2] \tag{8}$$

where g is the acceleration due to gravity, ΔT is the temperature difference between the surface and the height z (in degrees Kelvin), T_{abs} is the temperature of the air layer in degrees Kelvin, and Δu is the difference in wind speed between the surface and the height z. The constant σ in (7) has a value of 10.0 [*Webb*, 1970].

For lapse conditions we can write (G. Szeicz, personal communication, 1973)

$$(D_h)_u = D_h(1 - \sigma Ri) \tag{9}$$

where $(D_h)_u$ is the transfer coefficient for heat in unstable conditions. This case is unusual over snow, as was noted by *Fohn* [1973] and shown by *De la Casiniere* [1974]. In the present study the unstable case occurred only in 13 hours out of 17 days.

The only remaining undefined variable in the turbulent exchange equations is the roughness length z_0 in (6). This parameter is usually estimated by detailed measurement of wind profiles over the surface in question. This method is expensive, however, and gives highly variable results. Work by *Lettau* [1969] suggested an alternative approach whereby z_0 can be estimated from the height and cross-sectional area of surface forms. Lettau proposed

$$z_0 = h^* S/2S' \quad \text{cm} \tag{10}$$

where h^* is the effective obstacle height, S is the silhouette area in the downwind plane, and S' is the basal area of the obstacle.

The value derived for the snow surface by using this method was 0.5 cm. By means of this estimate of z_0 and the values of the relevant meteorological variables measured 2 m above the surface the turbulent heat flows into or out of the snow (H_e and H_c) may be defined. By means of a method described later to assess H_r, (1) can be solved, giving the total heat available for melting snow. No estimate was made of the thermal quality of the snow, and this was assumed to be 100%. This factor is unlikely to lead to significant errors.

TABLE 1. General Site Dimensions

Experimental Site	Forest Density	Area, m²	Mean Slope	Length, m	Aspect, deg
		Tundra			
A	0	2810	4°	85	242
B	0	1335	9°	49	271
C	0	1777	5°	37	58
		Woods			
D	0.162	2409	7°	85	62
E		1802	15°	54	215
F	0.164	1822	5°30′	61	13
G		1680	7°	76	244

EXPERIMENTAL SITES

The field work for this study was done near Schefferville, Quebec, Canada. The climate of the area is typical of the eastern Canadian subarctic, with only the months of July and August having mean temperatures above 10°C. The mean annual temperature is −4.7°C. May and June are the months when temperatures first rise above freezing. Annual snowfall is about 35 cm of water equivalent, approximately half of the average total annual precipitation.

The topography of the area is strongly structurally controlled into a series of north-northwest to south-southeast ridges, local relief being generally less than 200 m. The area is near the northern limit of tree growth, so that the boreal forest is restricted to the valleys and lower hillslopes, whereas the higher areas and ridges are covered by treeless tundra vegetation.

Seven experimental sites were constructed for the study. One

Fig. 1. General view of forest sites area.

group of four sites was in the boreal forest, and another group of three sites was on the tundra. Table 1 shows the site characteristics. The sites in each group were selected with a range of inclinations and aspects in order to have differing snowmelt environments. In the forest sites the tree canopy is discontinuous (Figure 1), with an areal coverage of about 16%, the two dominant tree species being black and white spruce. Tree heights range from 2 to 10 m. Underneath the canopy in most areas a dense underbrush of birch has developed. The forest floor is covered by a mat of lichens 5–10 cm thick, composed mainly of *Cladonia alpestris* (caribou moss). The lichen mat is not attached to the soil by roots. The roots of the underbrush are shallow, and even the roots of large trees penetrate less than 30 cm into the soil.

The soils in the forest are described [*Nicholson,* 1973] as minipodsols developed on dense silty glacial till. Because of its density and the lack of root holes the topsoil has low permeability in the unfrozen state and is essentially impermeable when it is frozen.

The tundra sites have no tree cover, although there are some dwarf spruce less than 1 m in height. The lichen mat, soils, and parent material on the tundra are very similar to those on the forest sites, except that both the lichen mat and the soil horizons are less well developed. The soils and tills in both groups of sites have a very low permeability, and in addition, during the snowmelt period they are heavily impregnated with 'concrete' frost [*Post and Dreibelbis,* 1942], which further reduces their permeability. Excavations made beneath the snowpack late in the season revealed no infiltration into the soil. Even under a thin snowpack late in the season the soil was so heavily frozen that a pickaxe was needed to penetrate the surface. The nature of the soils and the lack of subsurface runoff (see discussion later) demonstrate that infiltration into the frozen soil during snowmelt is negligible in the Schefferville area.

INSTRUMENTATION

At meteorological sites close to each group of runoff sites (forest and tundra) the following instrumentation was operated to monitor the energy balance of the snowpack.

1. In a clearing among the forest sites and also on the tundra, solar radiation in the open ($Q + q$) was measured using a Belfort actinograph. Both instruments were calibrated against an Eppley solarimeter.

2. A partial record of net radiation in the forest (H_{rf}) was measured by using five Funk-type net radiometers (3 weeks of data). Five instruments were used in order to obtain a good sample of net radiation in the forest, where there is substantial shading of the snow surface by trees. Net radiation was not measured on the tundra sites.

3. For 3 weeks a partial record of diffuse radiation in the open (q) was obtained near the wooded sites by using an Eppley solarimeter equipped with a shading band.

4. Hourly wind run at 2 m above the surface (u_z) was measured by using Cassella 3-cup, 8-cm recording anemometers, both in the forest and on the tundra.

5. Wet- and dry-bulb temperatures (T_a and T_w) were measured hourly at 2 m above the surface in the forest and on the tundra with a hand-held Assman aspirated psychrometer. This record of T_a and T_w was used in conjunction with standard meteorological tables to produce a record of atmospheric

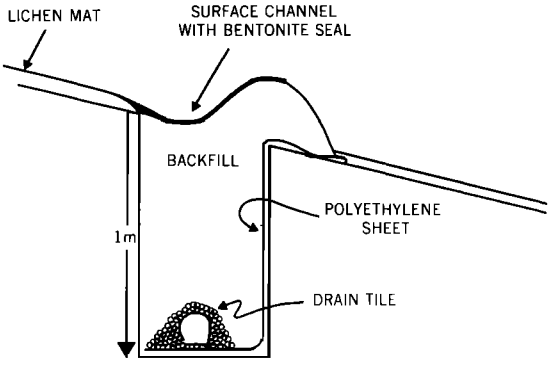

Fig. 2. Runoff interception instrumentation.

vapor pressure. When Assman readings were not available, the record was completed by using data from a Weather-Measure thermohygrograph placed in a Stevenson screen 2 m above the surface. The thermohygrograph readings were compared with simultaneous psychrometer readings and showed no significant differences.

6. Runoff from each plot was collected in a system like that shown in Figure 2. Water from the surface channel and the subsurface drain was led through pipes to weirs and recorded continuously. Because of the persistence of frozen soil under the snow, however, no subsurface runoff occurred until the end of the snowmelt period.

By means of standard techniques of hydrograph separation, daily melts in centimeters of water equivalent were derived from the runoff record. Daily melt totals are shown in Figure 3. The maximum daily melts observed on the four forest sites were 5 cm on site D, 2.7 cm on site E, 5.9 cm on site F, and 4.9 cm on site G. The low maximum value on site E is a result of the earlier breakup of the snowpack on this site. The breakup occurred before the days of highest energy input (twelfth and thirteenth days of the thaw), which gave high melts on the other slopes that still had complete snow covers.

Application of the Heat Flow Model

The application of the model required some further analysis and the use of an approximation. Each of the terms on the right-hand side of (1) can vary with local conditions of topography and cover; therefore seven snowmelt sites with differing inclinations and aspects under two cover types were selected so as to provide contrasting snowmelt environments.

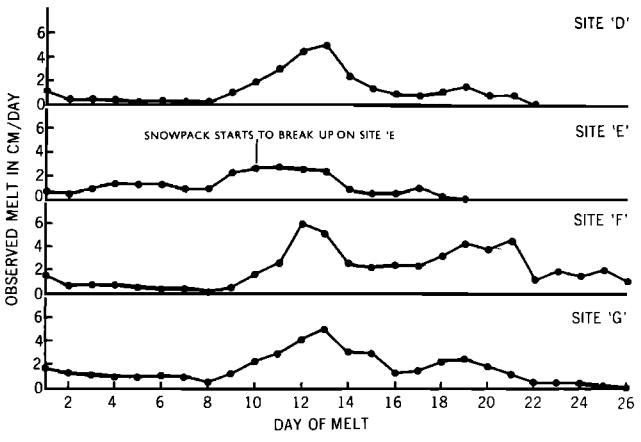

Fig. 3. Observed melts for the forest sites.

The most conspicuous variations in the energy balance are caused by differing vegetation types. The presence of trees reduces the amount of shortwave radiation reaching the snow surface. Trees, by reducing the wind speed, also reduce the exchanges of latent and sensible heat fluxes between the snow and the air. Both of these variations are included in the computed energy balance.

Another variation in the energy balance is that caused by the effects of slope inclination and aspect on the income of solar radiation. An analysis of this variation is given by *Garnier and Ohmura* [1968]. From a knowledge of direct and diffuse radiation fluxes on the horizontal, with slope inclination and aspect, longitude, latitude, and solar declination as inputs, total global radiation on a slope can be estimated. Unfortunately, diffuse radiation is not a commonly measured variable and was not available for the period considered in this paper. Following *Liu and Jordan* [1960] an estimate of diffuse and direct components of solar radiation was made from the short record of diffuse flux measured in 1972. Details are given by *Price* [1975]. The final result is an hourly record of global radiation on slopes of differing inclination and aspect. The analysis in the present paper showed that variations in the Schefferville area are generally small, although they become important for detailed modeling of runoff from individual hillslopes, particularly in the steeper areas. Figure 4 shows the differences in the income of global radiation between sites D (with a northeasterly aspect) and E (with a southwesterly aspect) on a day with high insolation. On such a day the direct-beam component is high, and so differences of insolation between the slopes are considerable. The peak rate of radiation income on site E is 15% higher than that on site D, and the daily total is 13% higher. In addition, the peak of incoming radiation is 2 hours later on slope E. This difference in timing is of interest when the generation of runoff from the snowpack is considered [*Dunne et al.*, 1976].

It was noted earlier that net radiation is not a routinely measured variable and that attempts to calculate H_r from its components were unsuccessful. *Petzold and Wilson* [1974] showed that net all-wave radiation over snow in the boreal forest of the snowmelt sites (D and F) could be derived from a linear regression of net radiation in the forest (H_{rf}) on global radiation in the open ($Q + q$). The relationship was

$$H_{rf} = -1.0 + 0.242(Q + q) \quad \text{cal cm}^{-2}\,\text{h}^{-1} \qquad (11)$$

$$r = 0.90$$

$$\sigma_e = 2.1 \text{ cal cm}^{-2}\,\text{h}^{-1}$$

$$n = 267$$

For an open melting snow surface like that on the tundra, *Petzold* [1974] showed that a relationship existed between net

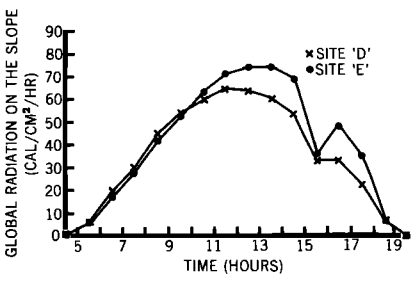

Fig. 4. Sites D and E, global radiation on a day of high insolation.

radiation in the open (H_{ro}) and global radiation in the open ($Q + q$) such that

$$H_{ro} = -0.60 + 0.150(Q + q) \quad \text{cal cm}^{-2}\ \text{h}^{-1} \qquad (12)$$

$$r = 0.84$$

$$\sigma_e = 2.4 \text{ cal cm}^{-2}\ \text{h}^{-1}$$

$$n = 107$$

The value of H_r under the two types of cover can therefore be calculated directly from measurements of solar radiation in the open. When they are used in conjunction with the Garnier-Ohmura mapping method, (11) and (12) allow the mapping of net radiation without direct measurement at each site.

Another factor which varies with environment is the wind speed at 2 m. On the three tundra sites a single anemometer was adequate to measure the wind speed for all three sites because of the lack of obstructions, but in the forest, wind speed at 2-m height on any site is a function of exposure, wind direction, tree spacing, and tree height. This spatial variation of wind speed between sites was assessed by placing one anemometer at the central meteorological site in the forest and one at the center of each of the four sites (D, E, F, and G). Wind run was measured for 15 days, and the results show that the wind speeds on the sites were generally less than those measured at the central station. A reduction of 10% was observed for site D, and one of 20% for sites E, F, and G. There is some uncertainty about the real values of wind speed on the sites, because of the variability of exposure with wind direction. The reduced wind speeds were used in the computation of the energy balance for the individual sites.

In order to apply the heat flow model on a 24-hour basis an approximation had to be used for the nighttime period. During the day, when the snow surface was known to be melting, the values of surface temperature (T_s) and vapor pressure (e_s) were fixed at 0°C and 6.11 mbar. At some point during the day the heat balance of the snowpack becomes negative, and the surface freezes. The following day, when sufficient positive heat flows have occurred to satisfy the heat deficit, the surface will start to melt again. Thus the periods for which $T_s = 0$ can

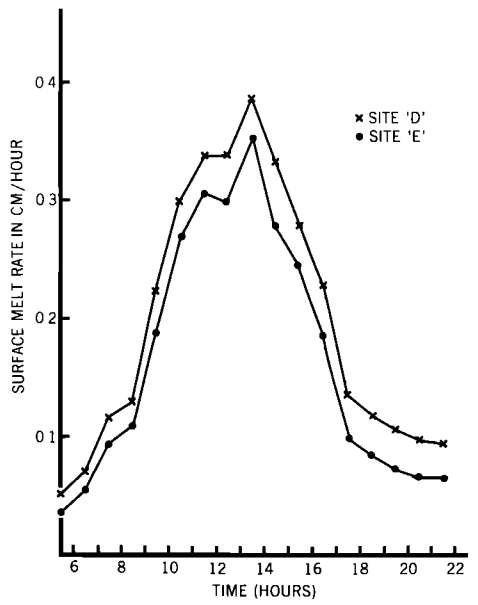

Fig. 5. Sites D and E, surface melt rates on a day of predominantly turbulent melt.

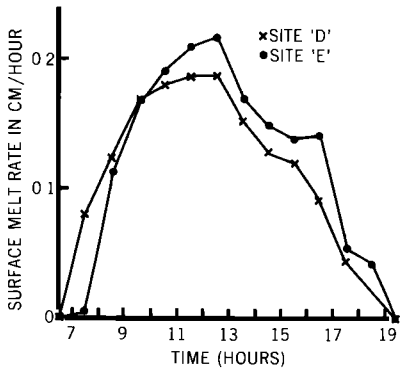

Fig. 6. Sites D and E, surface melt on a day of predominantly radiative melt.

be separated by observing the first freezing at night and the first melting in the morning. In the interim, T_s is not constant, and the surface will maintain equilibrium with the air, acting as a ventilated ice surface. Under ideal conditions (no radiative heat transfer), surface temperatures should then be equivalent to the wet-bulb temperature, and vapor pressure to the saturated vapor pressure over ice at the wet-bulb temperature. This approximation is equivalent to assuming that at night there is no net flow of heat into or out of the snowpack due to turbulent exchanges.

The times at which the surface froze at night and the time of first melt the next day were assessed visually in the field. These times are therefore not exact, so that there are short periods during many days when the value of T_s is not well defined, leading to uncertainty about the sign and magnitude of H_c and also about whether Ri is positive or negative. This uncertainty led to the computation of spuriously high negative sensible heat flows on a few occasions around the time of transition from $T_s = 0$°C to $T_s = T_w$. These values were caused by the incorporation of the correction factor (equation (9)) for negative Ri. Because of this and because the negative Ri conditions occurred only on 13 hours out of 17 days and always around the time of estimation of T_s, no attempt was made to correct negative sensible heat flows for stability, conditions being assumed to be neutral.

At night, negative heat flows can take place. Some sensible heat loss occurs from the pack, but this is unusual, occurring only 3% of the time. The main nocturnal losses are radiative. These radiative losses, predicted by (11) and (12), are accumulated into a heat deficit, which must be satisfied by the first positive flows of the next day, before any free water can be produced.

Results and Discussion

The model described above was used to predict melt rates for the seven snowmelt sites. Differences in vegetation cover, topography, and exposure combined to give different magnitudes and temporal patterns of melt on each site. Figure 5 shows the surface melt on sites D and E in the forest on a day of high turbulent heat flows. Because wind speeds were consistently higher on site D, this site has higher rates of melting throughout the day. Because the diffuse component of solar radiation was dominant on this day, there are no radiation-induced differences in surface melt. Figure 6 shows melt on the same two sites on a day of mainly radiative melt, with the skies being cloudless and with the direct component of solar radi-

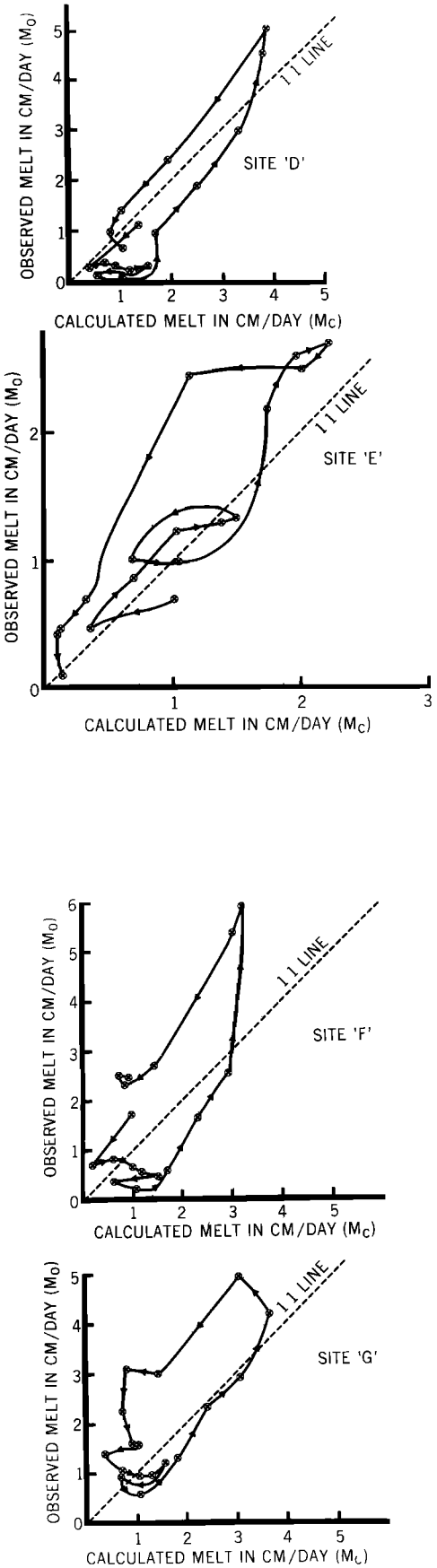

Fig. 7. Observed and calculated melt (M_o and M_c) for the four forest sites.

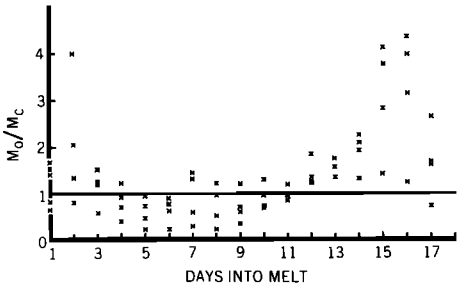

Fig. 8. Values of M_o/M_c for all forest sites.

ation being dominant. It can be seen that site D had higher melt rates in the early morning, when it intercepted more radiation than site E by virtue of its northeasterly aspect, but in the middle of the morning the situation was reversed, and site E intercepted more radiation than site D and had higher melt rates.

Some differences in the heat budget between the tundra sites and the forest sites are also of interest. The major differences are in the relative sizes of the three energy balance components. For a period of 7 days in 1972 the mean wind speed measured at the tundra meteorological site was 2.1 times greater than that at the forest sites. When equal air temperatures and surface roughnesses are assumed, this would cause (from (6)) a doubling of the turbulent exchange of sensible heat. For example, on one day of high melt rates on tundra site A, total melt due to sensible heat was 3.04 cm, whereas on forest site D it was only 0.94 cm. The reverse is true for net radiation. On the same day, total radiative melt was 1.05 cm on tundra site A and 1.50 cm on forest site D. The greater importance of H_r on the forest sites is obvious from a comparison of (11) and (12). For the same amount of solar radiation, more net radiation is generated in the forest than over the open surface. It seems probable that the presence of trees causes this difference.

To test the heat flow model, daily runoff totals were separated from the site hydrographs by plotting the recession limbs of the daily hydrographs on semilogarithmic graph paper and extrapolating the recession to isolate daily flows. This standard method of extrapolation suggested very long recessions, extending for up to 60 hours after the peak flow. The validity of extending recessions for such long periods was confirmed by using a physical model of flow through snow [*Dunne et al.*, 1976].

The heat flow model was used to predict total daily melts, and Figure 7 shows the relationship between observed melt (M_o) and calculated melt (M_c). The results shown are for the forest sites only, because leaking runoff collectors made the runoff measurement from the tundra sites unreliable. Two points are apparent. First, on sites D and E the predictions are good, and on sites F and G they are relatively poor. Second, the general pattern of prediction is very similar for all four sites. Site E is the only site on which the snow cover broke up appreciably during the period being considered, and the pattern of prediction on that site differs slightly from that on the other sites as the result of the application of a correction for the areal extent of the snowpack.

On all the sites the pattern of prediction is in the form of a 'hysteresis' loop, with overprediction occurring in the early melt season and underprediction in the late melt season. Although the estimates of the daily totals are good, the uniformity of the 'loop' pattern warrants some attention.

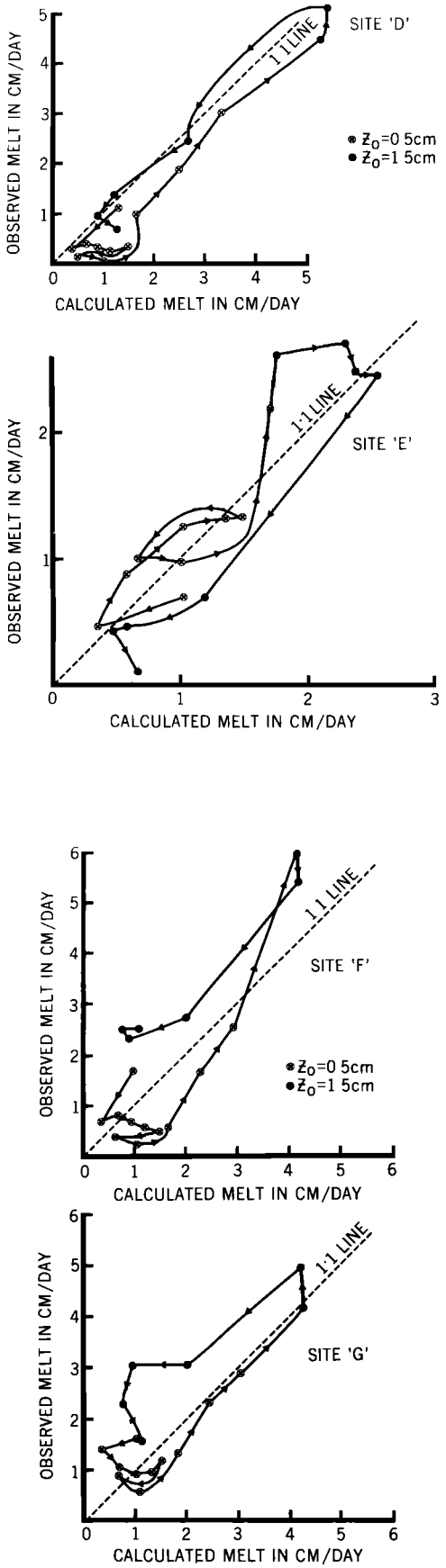

Fig. 9. Observed and calculated melt on the forest sites, with changing roughness length.

The source of error might be in either observed or calculated values of daily melt. Although the method of separation of daily flows was checked by using a physical model, it is still difficult to fit long recessions. Even small differences in the calculated recession rates can lead to differences in the separated runoffs of up to 0.5 cm/d. This may explain some of the differences between M_o and M_c, but there seems to be no reason why the error should be distributed in the way shown in Figure 7 for all sites. It is also possible that the observed values of runoff derived from the slope hydrographs may have been affected by changes in the effective drainage area of the plots. This is very unlikely because the drainage areas would have to have changed simultaneously, in the same way, and by similar amounts on all the sites.

The discrepancies seem to be caused by errors in the daily runoff predicted by the heat flow model. Of the three components of heat flow (H_r, H_e, and H_c), only H_e is well correlated (positively) with the difference between M_o and M_c. Mean daily vapor pressure is also positively correlated with the discrepancies. The *Brunt* [1932] equation indicates that vapor pressure is one of the controls of net long-wave radiation, so it is possible that the regression equations (11) and (12) mask the effects of vapor pressure upon net radiation. This was tested by using constants for the Brunt equation taken from work by *Sellers* [1965]. Using an air temperature of 10°C, vapor pressure was allowed to vary from 4 to 8 mbar, the observed change from the first day to the last day of the thaw. This doubling of e_a produced a change in calculated melt of approximately 0.4 cm/d. Changes in vapor pressure might therefore have been a factor contributing to the consistent hysteresis pattern in Figure 7, but since maximum differences between observed and calculated melts are of the order of 2 cm/d, vapor pressure changes cannot explain all of the discrepancies.

Two further features of the radiation estimate are possible sources of error. *Dunne and Price* [1975] show that the slope of lines describing the relationship between daily totals of H_r and $(Q + q)$ can increase with higher ambient air temperature, so that the amount of net radiation generated at any specific income of global radiation will be greater with higher air temperatures. This temperature-induced effect would cause (11) to underestimate H_r on warmer days, later in the melt. This may, again, explain some of the poor prediction, but we do not have data on this effect for the Schefferville sites. Finally, (11) was developed over an unbroken, relatively clean snow surface. Late in the thaw the accumulation of spruce needles, dust, lichen fragments, and birch leaves and also protruding vegetation tend to reduce the albedo of the snowpack. This change in conditions from the period when (11) was developed would again lead to the underestimation of H_r and M_c and could be masked by the average relationships expressed by the regression equations.

The most likely explanation of the difference between calculated and measured melts can be found by observing changes in the snow surface through the melt. Figure 8 shows the ratio of M_o/M_c for all sites through the melt. The predictions of the model obviously deteriorated late in the melt season. The value of roughness length (z_o) used in (6) was estimated from snow surface features. Although detailed observations were not made, it is known that on site E on the ninth day of the melt and on sites D, F, and G on the twelfth day the underbrush started to break through the snow surface. The underbrush is compressed flat to the ground by falling snow and recovers during the thaw, when the snow thins enough for the

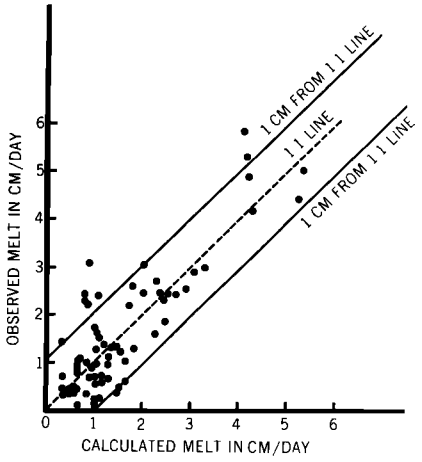

Fig. 10. Overall prediction on all forest sites.

branches to rise through the surface. At their early stages of exposure they protrude 10–15 cm over the snow and constitute a new roughness element. If the roughness length of this new element is taken as one tenth of the vegetation height [*Tajchman*, 1971], z_0 will be increased from 0.5 to 1.5 cm. This, in turn, increases the turbulent exchanges by about 50%. Figure 9 shows the revised estimates for those days when the surface of the snow had been broken by the underbrush; when z_0 is taken as 1.5 cm, the agreement is now much improved. Vegetation is even more exposed during the last few days of the melt, and the roughness of the surface will continue to increase. As the melt progresses, therefore, the dominant control of aerodynamic roughness seems to shift from the larger surface hummocks, which decline in size through the melt season, to the smaller protruding vegetation elements.

Nevertheless, the pattern of discrepancies still persists. The remaining differences late in the season, particularly on sites F and G, can probably be attributed to changes in the actual radiation balance which occurred late in the thaw. The increasing dirtiness of the snow, the increase in air temperature with time, and the increase in atmospheric vapor pressure all probably contribute to the underestimation of H_r using (11) and (12). In addition, and this may be more important and very difficult to assess, as the snowpack thins, the absorption of solar radiation by the ground becomes important, as does the absorption of solar radiation by the bushes protruding through the snow, providing extra energy by conduction and long-wave radiation.

Figure 10 shows the overall prediction on all four forest sites, with the roughness length changing as was described earlier. The relationship between measured daily melt (M_o) and calculated daily melt (M_c), both being expressed in centimeters per day, is

$$M_o = 0.08 + 0.97M_c \quad \text{cm/d} \qquad (13)$$

$$r = 0.85$$

$$\sigma_e = 0.71 \text{ cm/d}$$

$$n = 68$$

The regression constant (0.08) does not differ significantly from zero at the 5% level, and the regression coefficient does not differ significantly from 1.0, also at the 5% level. This relationship between observed and predicted values of daily snowmelt for small plots is quite satisfactory and is within currently accepted limits in snowmelt hydrology. It demonstrates that the physically based, spatially varied energy balance, incorporating corrections for stability of the air over the snowpack, is a good short-term predictor of snowmelt. The results suggest that future studies of snowmelt should concentrate upon changes in the snow surface during the melt period, particularly upon nocturnal surface temperatures, changing roughness, and variations in the radiation balance.

NOTATION

C_p specific heat of air at constant pressure, cal/g/°C.
D_h transfer coefficient for heat, cm h^{-1}.
D_w transfer coefficient for moisture, cm h^{-1}.
$(D_h)_s$ transfer coefficient for heat under stable conditions, cm h^{-1}.
$(D_h)_u$ transfer coefficient for heat under unstable conditions, cm h^{-1}.
e_a vapor pressure of the air at 2 m, mbar.
e_s vapor pressure of the surface, mbar.
g acceleration due to gravity, cm h^{-2}.
h^* effective obstacle height, cm.
H_c sensible heat flow, cal cm^{-2} h^{-1}.
H_e latent heat flow, cal cm^{-2} h^{-1}.
H_g ground heat flow, cal cm^{-2} h^{-1}.
H_m heat available for melting snow, cal cm^{-2} h^{-1}.
H_p precipitation heat flow, cal cm^{-2} h^{-1}.
H_r radiation heat flow, cal cm^{-2} h^{-1}.
H_{rf} net radiation in the forest, cal cm^{-2} h^{-1}.
H_{ro} net radiation in the open, cal cm^{-2} h^{-1}.
k von Karman's constant.
L latent heat of vaporization of water, cal g^{-1}.
L_n net long-wave balance, cal cm^{-2} h^{-1}.
$L\downarrow$ sky emission, cal cm^{-2} h^{-1}.
$L\uparrow$ emission from snow surface, cal cm^{-2} h^{-1}.
M_c calculated melt, cm/d.
M_o observed melt, cm/d.
p atmospheric pressure, mbar.
q diffuse fraction of solar radiation, cal cm^{-2} h^{-1}.
Q direct beam component of solar radiation, cal cm^{-2} h^{-1}.
Ri Richardson number.
S silhouette area in the downwind plane, cm^2.
S' basal area of the obstacle, cm^2.
T_a air temperature at 2 m, °C.
T_s temperature of the surface, °C.
T_w wet-bulb temperature at 2 m, °C.
T_{abs} mean air temperature, °K.
u_z wind speed at 2 m, cm h^{-1}.
z height of measurement, cm.
z_0 roughness length, cm.
α shortwave reflectivity (albedo).
σ empirical constant.
σ_e standard error of the estimate.
ρ_a density of air, g cm^{-3}.

Acknowledgments. The study was carried out while the writers worked at McGill University, Montreal, Quebec. A.G.P. was supported by two National Research Council of Canada awards: a bursary and a postdoctoral fellowship. The work was financed by awards to T.D. from the National Research Council of Canada, Canada Department of the Environment, and the Iron Ore Company of Canada. Thanks are extended to R. G. Wilson and Don Petzold, who supplied the radiation data, and to G. Szeicz, who helped greatly with the energy balance equations and critically read the manuscript.

We would also like to thank F. H. Nicholson, Director, McGill Subarctic Research Laboratory, and all the friends who helped during the study, particularly Joe Burns, Jim Franks, Margaret Nicholson, and Don Petzold.

REFERENCES

Anderson, E. A., Development and testing of snowpack energy balance equations, *Water Resour. Res.*, *4*(1), 19–37, 1968.

Anderson, E. R., Energy budget studies, *U.S. Geol. Surv. Prof. Pap. 296*, 1954.

Brunt, D., Notes on radiation in the atmosphere, *Quart. J. Roy. Meteorol. Soc.*, *58*, 389, 1932.

Collins, E. H., Relationship of degree-days above freezing to runoff, *Eos Trans. AGU*, *15*, 624–629, 1934.

De la Casiniere, A. C., Heat exchange over a melting snow surface, *J. Glaciol.*, *13*(69), 55-72, 1974.

Dunne, T., and A. G. Price, Estimating daily net radiation over a snowpack, *Climatol. Bull. 18*, pp. 40–48, McGill Univ., Montreal, Que., 1975.

Dunne, T., A. G. Price, and S. C. Colbeck, The generation of runoff from subarctic snowpacks, *Water Resour. Res.*, *12*, this issue, 1976.

Fohn, P. M. B., Short-term snowmelt and ablation derived from heat- and mass-balance measurements, *J. Glaciol.*, *12*(65), 275–289, 1973.

Garnier, B. J., and A. Ohmura, Computation and mapping of the shortwave radiation on a slope, *J. Appl. Meteorol.*, *2*, 796–800, 1968.

Lettau, H., Note on roughness-parameter estimates on the basis of roughness-element description, *J. Appl. Meteorol.*, *18*(5), 828–832, 1969.

Liu, B. Y. H., and R. C. Jordan, The interrelationship and characteristic distribution of direct, diffuse and total solar radiation, *Solar Energy*, *4*(3), 1–19, 1960.

Monteith, J. L., Dew, *Quart. J. Roy. Meteorol. Soc.*, *83*, 322–341, 1957.

Nicholson, H. M., Pedological studies in a subarctic environment, M. Sc. dissertation, 248 pp., McGill Univ., Montreal, Que., 1973.

Petzold, D. R., *Solar and Net Radiation Over Snow, Climatol. Res. Ser.*, vol. 9, 77 pp., Department of Geography, McGill University, Montreal, Que., 1974.

Petzold, D. R., and R. G. Wilson, Solar and net radiation over melting snow in the subarctic, in *Proceedings of the 31st Eastern Snow Conference*, pp. 51–59, Ottawa, Ont., 1974.

Post, F. A., and F. R. Dreibelbis, Some influences of frost penetration and micro-climate on the water relationships of woodland, pasture, and cultivated soils, *Soil Sci. Soc. Amer. Proc.*, *7*, 95–104, 1942.

Price, A. G., Snowmelt runoff processes in a subarctic area, Ph.D. dissertation, 185 pp., McGill Univ., Montreal, Que., 1975.

Pysklywec, D. W., K. S. Davar, and D. I. Bray, Snowmelt at an index plot, *Water Resour. Res.*, *4*(5), 937–946, 1968.

Sellers, W. D., *Physical Climatology*, 272 pp., University of Chicago Press, Chicago, Ill., 1965.

Tajchman, S., Evapotranspiration and energy balances of forest and field, *Water Resour. Res.*, *7*(3), 511–523, 1971.

U.S. Army Corps of Engineers, Snow hydrology, summary report of snow investigations, 437 pp., North Pac. Div., Portland, Ore., 1956.

Webb, E. K., Aerial microclimate, *Amer. Meteorol. Soc. Agr. Meteorol. Monogr.*, *6*(28), 27–58, 1965.

Webb, E. K., Profile relationships: The log-linear range and the extension to strong stability, *Quart. J. Roy. Meteorol. Soc.*, *96*, 67–90, 1970.

Wilson, W. T., An outline of the thermodynamics of snowmelt, *Eos Trans. AGU*, *22*, 182–195, 1941.

Zuzel, J. F., and L. M. Cox, Relative importance of meteorological variables in snowmelt, *Water Resour. Res.*, *11*(1), 174–176, 1975.

(Received November 25, 1975;
accepted February 17, 1976.)